Contribution of Tore Supra in Preparation of ITER

B. Saoutic, on behalf of the Tore Supra Team

CEA, IRFM, F-13108, St-Paul-Lez-Durance, France

E-mail contact of main author: bernard.saoutic@cea.fr

Abstract: Tore Supra routinely addresses the physics and technology of very long duration plasma discharges, thus bringing precious information on critical issues of long pulse operation of ITER. A new ITER relevant LHCD launcher has allowed coupling to the plasma a power level of 2.7 MW for 78 s, corresponding to a power density close to the design value foreseen for an ITER LHCD system. In accordance with the expectations, long distance (10 cm) power coupling has been obtained. Successive stationary states of the plasma current profile have been controlled in real time featuring i) control of sawteeth with varying plasma parameters, ii) obtaining and sustaining a "hot core" plasma regime, iii) recovery from a voluntarily triggered deleterious MHD regime. The SOL parameters and power deposition have been documented during L-mode ramp-up phase, a crucial point for ITER before the X-point formation. Disruption mitigation studies have been conducted with massive gas injection, evidencing the difference between He and Ar and the possible role of the q=2 surface in limiting the gas penetration. ICRF assisted wall conditioning in the presence of magnetic field has been investigated, culminating in the demonstration that this conditioning scheme allows to recover normal operation after disruptions. Effect of the magnetic field ripple on the intrinsic plasma rotation has been studied, showing the competition between turbulent transport processes and ripple toroidal friction. During dedicated dimensionless experiments, the effect of varying the collisionality on turbulence wavenumber spectra has been documented, giving new insight into the turbulence mechanism. Turbulence measurements have also allowed quantitatively comparing experimental results to predictions by 5D gyrokinetic codes: numerical results simultaneously match the magnitude of effective heat diffusivity, rms values of density fluctuations, and wave-number spectra. A clear correlation between electron temperature gradient and impurity transport in the very core of the plasma has been observed, strongly suggesting the existence of a threshold above which transport is dominated by turbulent electron modes. Dynamics of edge turbulent fluctuations has been studied by correlating data from fast imaging cameras and Langmuir probes, yielding a coherent picture of transport processes involved in the SOL.

1. Introduction

Achieving long-duration high performance discharges in a magnetic fusion device is one of the most important challenges "en route" to a fusion reactor [1]. The mission of Tore Supra, as the largest super-conducting tokamak presently in operation (minor radius $a \leq 0.78$ m, major radius $R \leq 2.40$ m, plasma current $I_p \leq 2$ MA), is to investigate the physics and technology issues of steady state tokamak operation. Integrating all technologies necessary for long pulse operation (superconducting magnets, actively cooled plasma facing components, long pulse heating and current drive systems), Tore Supra offers unique capabilities to routinely produce long duration, high power discharges, as exemplified by the realization of discharges lasting more than 6 minutes with a total injected energy of 1GJ [2]. At a time when the importance of long pulse operation issues grows as ITER implementation progresses, such asset leads to focus more on more the Tore Supra programme towards support to ITER. This contribution of the Tore Supra programme will even be amplified with the completion of the ongoing lower hybrid current drive (LHCD) system upgrade (the CIMES project [3]) that will allow, not only to test technological objects in more stringent conditions but also to extend the operational domain of long-duration discharges to higher plasma current and densities.

This paper reports the main achievements of the Tore Supra programme in the last two years. Plasma tests of an ITER-relevant LHCD launcher, developed in the frame of the CIMES project, are reported in section 2. Section 3 deals with development of plasma controls, a key issue to routine long pulse operation, as well from the safety and reliability as from the plasma performance optimisation point of view. Section 4 describes specific experiments in direct support of ITER operation in the domain of plasma start-up, disruptions and conditioning in the presence of permanent magnetic field. Finally, section 5 presents more fundamental studies in which Tore

Supra comprehensive set of diagnostics allows to be at the forefront of the comparison between experiments and the state of the art modelling.

2. Characterization of the Properties of the Passive Active Multijunction Lower Hybrid Current Drive Launcher

In the frame of the enhancement of the LHCD system, known as the CIMES project [3], a new ITER-relevant LHCD launcher, based on the Passive Active Multi-junction (PAM) concept [4,5] has been built and brought into operation on Tore Supra. The PAM design offers two distinctive advantages in view of next step fusion devices: i) as will be required in ITER, it allows efficient cooling of the waveguides that will be heated by plasma radiation, RF losses and neutron damping; ii) it offers low power reflection close to the cut-off density (n_{co} = $1.7\times10^{17}m^{-3}$ at f = 3.7GHz), which is an asset for operation in ITER, where the large distance between the plasma and the wall may bring the density in front of the launcher to low values. A significant part of the 2009/2010 experimental campaign of Tore Supra was devoted to characterize the PAM launcher behaviour, notably to: i) assess its coupling properties, ii) demonstrate reliable power coupling during edge perturbations mimicking ELMs, iii) achieve ITER-relevant power density, i.e. $25MW/m^2$ at f = 3.7GHz [6], in pulse lengths several tens of seconds, iv) assess its current drive capabilities.

The power reflection coefficient (RC) behaviour on the PAM launcher (denoted C4) has been studied in dedicated coupling experiments carried out at low power (200kW, i.e. $\sim 2MW/m^2$) in order to avoid possible non-linear effects that can occur at high power [7]. The density at the launcher mouth was varied from $0.5\times10^{17}m^{-3}$ to $8\times10^{17}m^{-3}$ by varying the plasma-launcher distance during the pulse. Figure 1 shows the measured RC, averaged over the 16 modules, versus the electron density at the launcher mouth, as measured by Langmuir probes mounted on the launcher. As expected, a good coupling, i.e. RC < 2%, is obtained in the vicinity of the cut-off density. The two lines in Figure 1 correspond to calculations from the linear coupling code ALOHA [8]. This code takes into account realistic 3D antenna geometry and can cope with double electron density decay lengths (λ_n) in the scrape-off layer (SOL). The first density layer (λ_{n1} ~ mm) describes the private SOL between the side protections on the launcher, while the second density layer (λ_{n2} ~ cm) describes the main SOL. As can be seen in Figure 1, good agreement between experiment and modelling is obtained.

LHCD experiments were also carried out in the presence of edge perturbations, produced by supersonic molecular beam injection (SMBI) to simulate ELM-behaviour. During SMBI, the electron density in front of the launcher increases from $2\times10^{17}m^{-3}$ to $10\times10^{17}m^{-3}$ and the RC increases from 1.5% to 7% (see Figure 2), in accordance with the coupling code prediction.

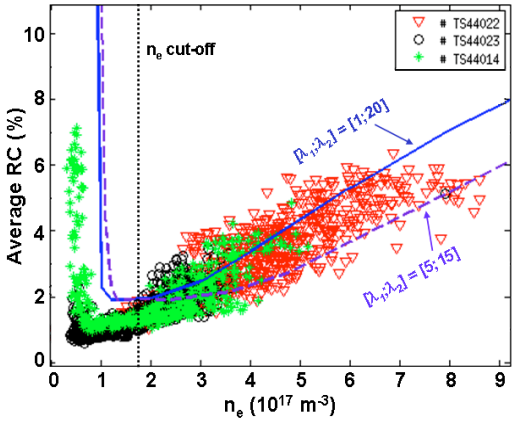

Figure 1: PAM launcher reflection coefficient vs. electron density at the launcher mouth.

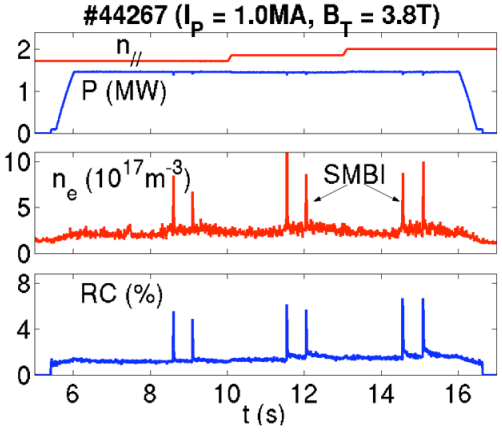

Figure 2: RC behavior during edge perturbations produced by SMBI.

At least at this power level (~1.5MW), the applied power remains constant during SMBI, indicating the possibility to couple during edge perturbations, such as ELMs. It has to be noted that the latest ITER PAM design [7] will allow less excursion in RC during an increase in density, making it a more ELM-resilient system.

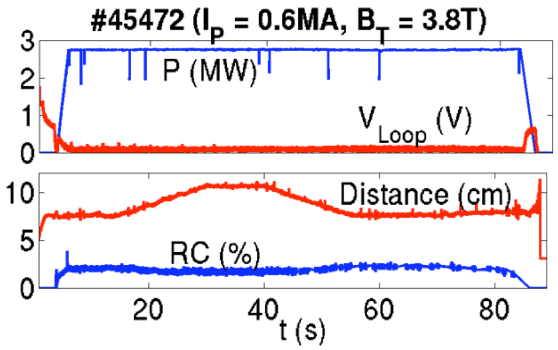

Figure 3: LHCD power, loop voltage (top); distance, reflection coefficient (bottom) vs. time.

The maximum power and energy coupled by the PAM launcher so far, after ~400 pulses on plasma, is 2.7MW during 78s (see Figure 3), corresponding to an injected energy of 210 MJ. This represents a power density of 25MW/m^2 consistent with the design value for an ITER LHCD system (33MW/m^2 at f = 5GHz and 25MW/m^2 at f = 3.7GHz) [6]. In addition, 2.7MW was coupled at a plasma-launcher distance of 10cm, with RC as low as 2%. It is worth noting that the maximum power coupling capability is probably higher than 2.7 MW, and that higher power experiments are foreseen in the near future when the new more powerful klystrons TH2103C (part of the CIMES project) will be operational on Tore Supra. During these high power experiments, the PAM concept also demonstrated its excellent cooling capabilities, with the temperature of the waveguides and the side protections, which are actively cooled, remaining below 300°C.

The intensity of the fast electron beams accelerated in near field of the waveguide rows the launcher was also investigated by detailed radial-poloidal mappings using a retarding field analyser, as described in [9]. The first results seem to indicate that the parasitic electron beam is less intense with the PAM launcher, compared to what was previously observed with a FAM launcher under similar experimental conditions [9]. This result remains however to be confirmed in experiments with the PAM and FAM coupling power on the same plasma target.

Full non-inductive pulses lasting up to 50s have been performed with the PAM launcher, using real-time control loops to maintain the plasma current constant by adjusting the LHCD power and to maintain the primary flux consumption at zero by acting on the central solenoid voltage. P_{LH} = 2.2MW was required to maintain I_P = 0.5MA and V_{Loop} = 0 at $\bar{n}_e$ = 1.45×10^{19}m^{-3}. Parallel refractive index $n_{//}$ = 1.72 was used, which corresponds to the optimum value, i.e. giving highest power directivity on the PAM. The value of the current drive efficiency (i.e. $\eta_{CD} = \bar{n}_e R_0 I_{CD}/P_{CD}$, where I_{CD} is the current driven by LHCD and P_{CD} is the coupled LHCD power) was approximately 0.75×10^{19}m^{-2}A/W, taking into account a bootstrap current fraction of 10% (i.e. $I_{CD} = 0.9 \times I_P$). The current drive efficiency with the PAM is found to be comparable to that obtained with the fully active multijunction launchers, when using the same peak value of the $n_{//}$-spectrum, as for example in the GJ-discharges [2].

3. Advance in Real Time Control of Stationary States of Plasma

Plasma control is key to routine long pulse operation, as well from the safety and reliability as from the plasma performance optimisation point of view. Development of real time (RT) algorithms is thus an important part of the Tore Supra programme that has pioneered the necessary integration between safety control and plasma performance optimisation one [10]. This section reports recent progress with emphasis on current profile control by 'search and maintain' algorithms that require long pulse capability: indeed, in order to determine the proper feedback to the actuator, such algorithms need sufficiently long time step so that the current profile has fully relaxed before to proceed to the next step.

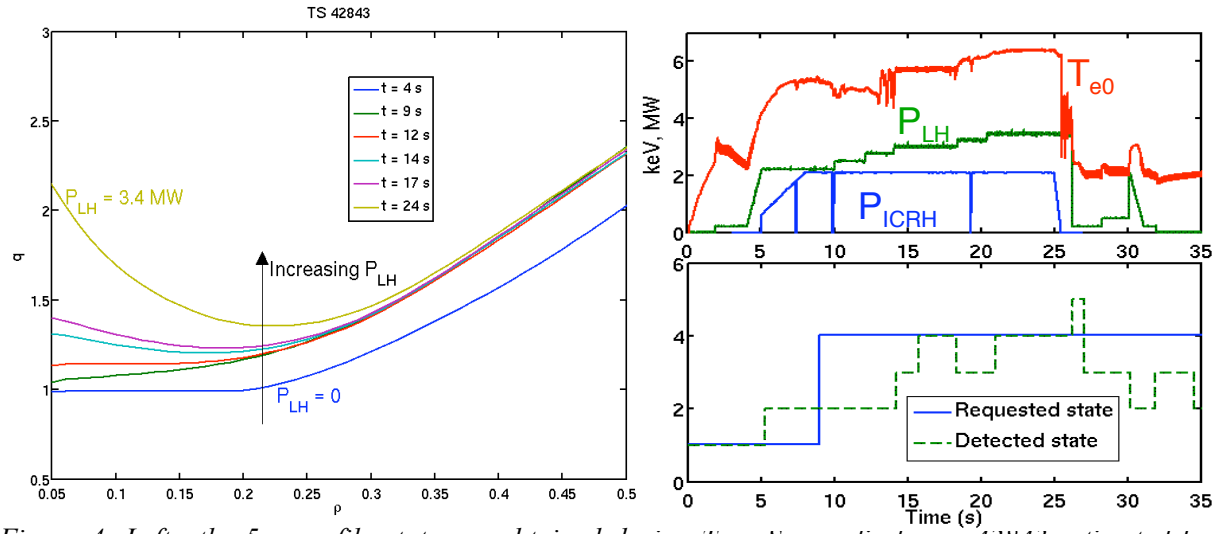

Figure 4: Left : the 5 q-profile states as obtained during Tore Supra discharge 42843 estimated by current diffusion simulation with the CRONOS code. Right : Time traces of various quantities. Top : central electron temperature from the ECE diagnostic (red), ICRH power (blue), LH power (green). Bottom : requested target q-profile state (solid blue) and detected by the control algorithm q-profile state (dashed green).

Real time control of stationary states of the current profile. The plasma current profile is controlled by varying the level of LHCD power, i.e. replacing part of the ohmic current by a non-inductive source with a different deposition profile. By increasing the LHCD power, the safety factor profile can thus be varied at will from a sawtoothing monotonic one to a mildly reversed profile with $q_{min} \sim 3/2$. In this range, the q-profile evolves through five distinct states, characterised by specific Magneto Hydrodynamic (MHD) activity: state #1, sawtooth with monotonic q profile and $q_0 < 1$ (t = 4s in Figure 4, left); state #2, no sawtooth with monotonic q profile and $q_0 \sim 1$ (t = 9s & 12s); state #3, small or large relaxation of the electron temperature (T_e), in relation with the q = 3/2 surface, with low or negative magnetic shear (t = 14 & 17s); state #4, high core Te with no visible MHD activity and reversed magnetic shear q_{min} being close to 3/2 (t = 24s) [11]; state #5, large MHD mode triggered at the q = 3/2 surface then coupled to the q=2 surface, a deleterious state known as the MHD regime [12]. The q-profiles states are detected by RT analysis of the T_e relaxations resulting from the MHD activity, observed on the central channels of the Electron Cyclotron Emission diagnostic (ECE). The operator specifies in advance the desired q-profile state as a function of time (the "target"). Then the control algorithm adapts the LH power in real time to follow the target. Every Δt seconds, the controller checks whether the plasma is in the requested plasma state and, if not, modifies the LH power in the relevant direction of a discrete step ΔP_{LH}. At the end of each P_{LH} plateau the current profile has reached its stationary state. Several experiments have been carried out on Tore Supra to demonstrate the capability of this control scheme i) to obtain a desired stationary q-profile state and ii) to sustain it in spite of preset variations of other plasma parameters such as plasma density, ICRH power or total current. Successful experiments have been carried out featuring i) control of the presence/absence of sawteeth with varying plasma parameters, ii) obtaining and sustaining a "hot core" plasma regime without MHD activity, iii) recovery from a voluntarily triggered deleterious MHD regime. Figure 4 displays discharge #42843 one of the most complete example of these control experiments, where the plasma goes through the 5 q-profiles states in a fully controlled way. The scenario of this experiment is i) to obtain a steady q-profile state #4 then ii) voluntarily trigger the MHD regime from this state by decreasing the ion cyclotron resonant heating (ICRH) power and iii) let the controller apply its emergency strategy to depart from the MHD regime and recover a usable plasma discharge.

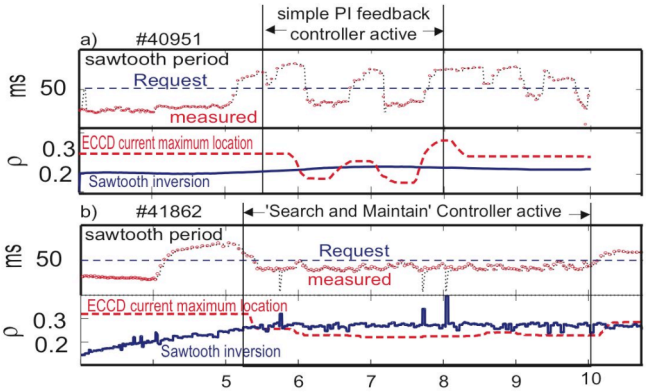

Figure 5: RT sawtooth period control with the poloidal injection angle as actuator: (a) using a PI controller; (b) using a search and maintain controller.

Real-time destabilisation of sawteeth by ECCD. Significant improvement in the RT control of fast ion stabilised sawteeth with electron cyclotron current drive (ECCD) has been obtained. To achieve the destabilisation of such sawteeth, the ECCD has to be localised in a fairly narrow range around the q=1 surface. In previous Tore Supra experiments, when scanning the ECCD location across the q=1 surface, by varying the ECCD injection angle, the sawtooth period exhibited a bi-stable behaviour, switching abruptly between long and short sawteeth. A first attempt was made to control the sawtooth period in real time, by using the difference between the requested and the measured sawtooth period as input to a proportional-integral controller. However, this resulted in oscillatory behaviour of the controller with the sawtooth period switching between the two obtainable values [13] (see Figure 5(a)). To solve this problem a more advanced 'search and maintain' algorithm has been developed. For the purpose of this algorithm, real time determination of the sawtooth inversion radius is added to the real time sawtooth period determination. The estimated location of the ECCD current is also determined in real time. This determination of the ECCD location is not based on any plasma measurement but it is based on lookup tables generated off line using the REMA code [14]. These lookup tables give the ECCD location as a function of the ECCD injection angles and the toroidal field. Knowing the sawtooth period, the sawtooth inversion radius and the ECCD location in real time, the algorithm starts by varying the ECCD injection angles and thereby the ECCD location, until sawteeth shorter than a reference value are obtained. Once short sawteeth are obtained, the controller memorises the ECCD location and the sawtooth inversion radius at this moment. Following this, the controller assures that the ECCD location tracks the sawtooth inversion radius, thereby maintaining short sawteeth throughout the ECCD pulse as can been seen on Figure 5(b). Using this scheme, 600 ms long sawtooth stabilized by 6 MW of ICRH power were shortened virtually down to ohmic level by 600 kW of ECCD. These experiment show that achieving and maintaining short sawteeth through RT controlled ECCD seems a viable option for NTM avoidance in plasmas where sawteeth are stabilised by significant fast ion pressures inside the q=1 surface.

Towards a plasma discharge flight simulator. The unique know-how developed on Tore Supra for safety and plasma performance real time control is being capitalized by developing, under the European integrated tokamak modelling framework, a plasma discharge "flight simulator", for control algorithm development. Two main modes of operation have been identified according to the step-by-step process needed to develop new control algorithms. The first mode is called "fully simulated". It is a non-intrusive method, which allows testing the controllers for any possible operation scenarios without using any subsystem of the tokamak. This mode of operation should also be used before any plasma discharge in order to validate the pre-pulse settings. The second functionality of the simulator consists in using the tokamak Plasma Control System (PCS) to run the feedback controllers; the plasma response is provided by plasma models. This mode of operation is called "hardware in the loop" as a part of the tokamak resources are used but without harming the machine to be controlled. More generally, the plasma flight simulator can be used to develop and test any RT algorithms such as the processing of the diagnostic raw data to provide "high level" physics information.

The originality of the project is to perform the plasma and feedback control simulation using as much as possible the tools developed under the European Integrated Tokamak Modelling (ITM) [15] task force. This feature allows to benefit from the developments of plasma models performed under the ITM task force and to define a flexible plasma simulation that can be adjusted on demand to the simulation needs. The architecture for the simulator has been defined. It consists of ITM applications, and a workflow engine in charge of the plasma models scheduling based on Kepler [16]. The development of controllers has to be performed under a friendly environment by a tool providing high-level development functionalities. The freeware ScicosLab [17] has been chosen because it is an integrated environment capable of designing and simulating digital controllers and offering automatic C code generation that can be used either as a Kepler actor under the European simulation platform or in the tokamak PCS. Interfacing the control toolbox ScicosLab with the Kepler framework has begun with the demonstration that a basic controller developed under the ScicosLab tool can be automatically converted to a C code and used as an actor in the Kepler framework. It is worth to note that, if such developments benefits from the ITM works, it also contributes to ITM by revealing new requirements.

4. Preparing ITER Operation

Tore Supra offers many feature that are common with ITER, as a permanent magnetic field present between discharges, actively cooled plasma facing components (PFC), long pulse heating and current drive systems… This naturally led to devote, during the last two years, a significant part of the Tore Supra programme to experiments in direct support of ITER operation.

Determination of Scrape off Layer Parameters during L-mode Ramp-up Phase. A crucial point for ITER first wall design, is the determination of the scrape off layer (SOL) parameters and power deposition during the L-mode ramp-up phase of ITER before the X-point formation, during which the plasma will have a circular cross-section and will be leaning directly on the beryllium tiles of the first wall. Present design work refers to the ITER physics basis [18] which proposes a scaling law for λ_q which is derived from L-mode plasmas in X-point divertor tokamaks : $\lambda_q = (1 \pm 1/3) \times 3.6\ 10^{-4}\ R^2\ P_{SOL}^{-0.8}\ q_a^{0.5}\ n_e^{0.9}\ Z_{eff}^{0.6}$. In order to check this scaling in limiter configuration, dedicated experiments were carried out in Tore Supra in order to measure SOL parameters in a controlled series of discharges that explore the control parameters of the scaling law proposed for ITER limiter plasmas. These experiments were conducted with plasma lying on the high field side (HFS), as it is the preferable scenario because blobby SOL transport leads to broader decay lengths and lower separatrix heat fluxes as compared to low field side (LFS) contact points [19,20]. The parameter ranges obtained were $0.04 < P_{SOL} < 0.71$ MW, $3.4 < q_a < 11.5$, and $0.3 < n_e < 4.9\times10^{19}$ m^{-3}. The parameters were fairly well decoupled from one another by doing a series of plasma current ramps for different fluxes of injected gas, and for several values of magnetic field $2.4 < B_T < 3.8$ T. When comparing the measured λ_q with the scaling law prediction, a significant scatter is observed: 108 measurements (out of 186) lie outside allowed uncertainty of ±50% (see Figure 6). Analysis of the data shows that the scatter is not due to random experimental errors, but instead to different trends than those predicted by the scaling law. For example, the measured λ_q decreases with density, whereas the scaling law predicts the opposite

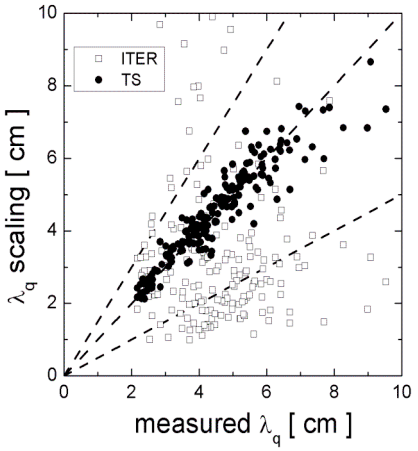

Figure 6: measured λ_q in the SOL compared with the ITER scaling law (open square) and the Tore Supra fit (solid circle).

behaviour. Careful visual inspection of the Tore Supra data set shows that the measured profiles are very reproducible for a given set of macroscopic parameters, even when the experiments are separated by intervals of several years (the oldest and newest measurements were made in 2004 and 2009 respectively). All the measured λ_q with HFS contact point, without exception, can be very well fitted by a simple empirical expression: $\lambda_q = (1 \pm 1/10) \times 0.025\ P_\Omega^{-0.8}$ (see Figure 6). In light of the differences between Tore Supra measurements and the L-mode scaling law, we suggest that similar experiments be carried out in other tokamaks in order to derive a sound scaling law for extrapolation to ITER. Most crucially, the strong scaling with tokamak major radius needs to be verified.

Disruption and Runaway Studies. Disruptions and runaway electrons (RE) are identified as a major issue for ITER and reactor-size tokamaks. Disruption produces excessive heat loads on plasma facing components, induces strong electromagnetic forces in the vessel structures, and generates multi-MeV runaway electrons. Thus mitigation techniques are strongly mandatory to minimize disruption and RE effects on PFC. Massive gas injection (MGI) prior to thermal quench and/or during the current quench is one of the proposed methods studied on Tore Supra. Several different injection scenarios on stable plasma were performed using different gases in various amounts. This included Helium (He), Neon (Ne), Argon (Ar) and a He/Ar mixture (95%/5%), with amount of gas injected ranging from 5 to 500 Pa.m^3. The photo-neutron production is used as an indicator of the amount of RE hitting the wall. Figure 7 displays the results of these experiments. He-mitigated disruptions showed a strong reduction in runaway production. For injection ranging from 20 to 500 Pa.m^{3}N, no dependence to the amount injected is observed. Only with 10 Pa.m^3 He injections, a few RE are sometimes produced. He/Ar mixture is as efficient as pure He. Conversely Ar and Ne does no prevent runaway generation. Ar generates even more runaways with increasing amounts of injected gas. Eddy currents in the toroidal pumped limiter (TPL) are moderately reduced by all the gases, and are rather more dependants on the time constants of the structures than on the gas species. In order better understanding the MGI results, the fuelling efficiency and gas penetration dynamic has been investigated. Due to its higher speed velocity, light gas penetrates quicker, and the density rise is steeper. Helium adds at least 3 times more free electrons (up to 2.10^{21}) to the plasma than Ar ($\sim 0.5\ 10^{21}$). Finally the thermal quench (TQ) is triggered at much higher density with He than Ar. This efficiency difference and the corresponding higher density reached at TQ likely explain the RE suppression when using light gases. The cold front speed inside the plasma, inferred from a fast framing visible camera, ranges from 20 m/s for weak Ar injection to 120 m/s for large helium injections. On the contrary the penetration depth seems to be independent of the nature and amount of gas. The gas jet is seen to be blocked along or near the q=2 flux surface, whatever the plasma temperature and/or the current profile are. Detailed analysis of the fast imaging system, of the soft X-ray diagnostic and of the Mirnov coils [21] support the following mechanism: when reaching the vicinity of the q=2 surface, the cold front triggers a large MHD activity that expels energy from the core; all the neutral gas near the q=2 surface is ionized thus preventing further penetration of the neutrals until the disruption occurs. Such observations bring important insight to the mechanism being at work during MGI, a necessary input for further simulation and extrapolation to larger devices like ITER.

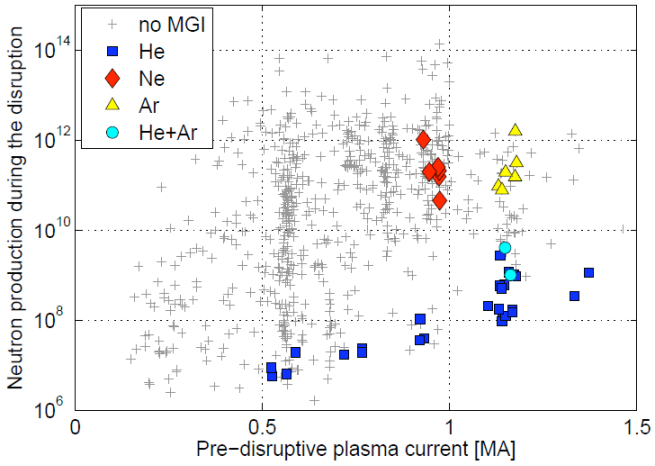

Figure 7: photo-neutron production vs. pre-disruptive plasma current for various MGI scenarios.

ICRH assisted Wall Conditioning. For the operation of ITER and future superconducting fusion devices, the presence of a permanent toroidal magnetic field will prevent the use of conventional glow discharge conditioning (GDC). A promising alternative makes use of discharges created with RF power in the ion cyclotron range of frequency, which are fully compatible with the presence of the magnetic field. The Ion Cyclotron Wall Conditioning (ICWC) technique was recently approved for integration into the ITER baseline using the ITER ICRH system. However, new investigations are needed prior to its validation and its application to ITER, in particular for recovery after disruptions, isotopic ratio control and fuel removal. Thanks to the long pulse capability of Tore Supra sub-systems, it was possible comparing the effect of continuous and pulsed ICWC discharges. ICWC discharge where performed with duration ranging between 1 and 60 seconds and coupled power ranging between 25 and 250 kW. Helium, hydrogen (H) gases and He/H gas mixture were injected either at constant rate or trough feedback control on the pressure in the torus. Continuous ICWC discharges appears to be more efficient for isotopic ratio control of the wall and fuel removal: using a He/H gas mixture, the isotopic ratio H/(H+D) evolves from 4% just after preloading of the wall by Deuterium (D) GDC to 50% after nearly 900 seconds of ICWC discharges cumulated duration. However, particle balance analysis reveals that H retention ($3.2\ 10^{22}$) is on average ten times higher than D exhaust ($3.4\ 10^{21}$). Short ICWC pulses, followed by sufficient pumping time (30 seconds in these experiments), have to be used to reduce the H retention over a discharge and post-discharge cycle. In order to optimize the fuel removal efficiency, the effect of ICWC pulse duration has been studied. Figure 8 displays the results, showing that the ratio between D outpumping and H retention can be reduces to unity for sufficiently short pulse duration (~1 second) without severely decreasing the D removal. Pulsed ICWC discharges have also been successfully used for recovering normal operation after disruptions, in a situation where, due to wall saturation, subsequent plasma initiation would not have been possible without conditioning. Following a disruption, provoked during an ohmic discharge at a plasma current of 1.2 MA (current decay rate 360 MA/s), it was checked that subsequent plasma initiation was not possible. Pulsed ICWC discharge was then applied (He gas, torus pressure 4.10^{-2} Pa, coupled RF power 60 kW, 2 seconds long pulse every 10 seconds applied 10 time) and allowed successful recovery of normal operation. This procedure was successfully repeated. It is worth to note that the HD partial pressure in the torus ($2\ 10^{-3}$ Pa) and HD molecule removal rate ($\sim 10^{16}$ $s^{-1}m^{-2}$) in ICWC was found comparable with those obtained in Taylor like pulsed discharges [22], which are routinely used on Tore Supra to recover from disruptions.

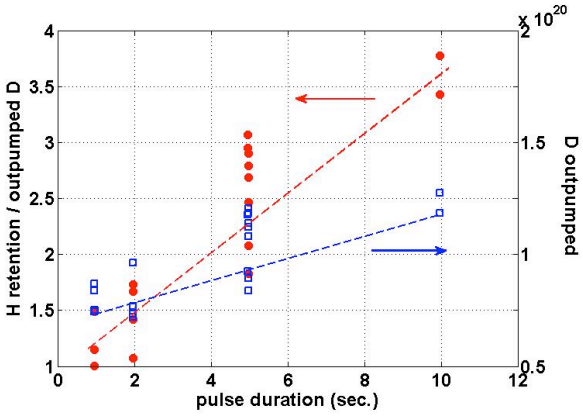

Figure 8: D outpumping (open square) and ratio of retained H over D outpumping (solid circle) vs. ICWC pulse duration (H gas, P_{RF}~100 kW, p ~10^{-2} Pa).

5. Fundamental Physics Studies

Supported by a strong modelling programme, a substantial part of the Tore Supra experimental time has also been devoted to physics oriented investigation.

Influence of Magnetic Field Ripple on the Intrinsic Plasma Rotation. Plasma rotation is considered to play a key role in tokamak plasma performance. Nevertheless, in a fusion reactor or ITER, no strong external momentum source is expected. Thus, there has been a

growing interest in the intrinsic rotation of plasma, i.e. without external momentum injection. However an effect that is still to be accounted for, when extrapolating intrinsic rotation observations to ITER, comes from the influence of magnetic field ripple (MFR). In order to document this phenomenon, dedicated ohmic L-mode experiments have been conducted on Tore Supra, by varying the plasma size while keeping the edge safety factor constant, thus allowing to scan the MFR amplitude δ_a from 0.5% to 5.5% at the plasma boundary. The toroidal velocity (V_Φ) radial profiles have been measured using a Charge eXchange Recombination Spectroscopy (CXRS) system [23]. For the low ripple case (δ_a = 0.5%), the whole plasma rotates in the co-current direction and the profile is peaked. When increasing the edge δ_0, the profile progressively shifts towards counter rotation: for δ_a = 1.62%, the plasma counter-rotates in the edge region ($\rho > 0.6$) while the core region is still co-rotating; for the highest ripple case (δ_a = 5.5%), the whole plasma is counter-rotating. This behaviour is consistent with observation on JET [24] and JT-60U [25]. A coherent picture is obtained when plotting for the whole δ_a scan, the measured V_Φ versus δ_{loc}, the local value of the MFR amplitude at the CXRS measurement location (see Figure 9): V_Φ is continuously decreasing with δ_{loc}, evolving from co-rotation to counter-rotation and approaching, for the largest δ_{loc}, level of neoclassical predictions accounting for the ripple induced thermal toroidal friction [26]. This observation strongly suggests a competition between two mechanisms. Indeed, when considering only ripple induced toroidal friction, the rotation should always be in the counter-current direction. At high ripple amplitude, the ripple induced thermal toroidal friction is dominating while at low ripple amplitude turbulent transport processes are likely the main drive for rotation. The scatter in V_Φ observed for $\delta_{loc} < 0.5$ would then be explained by different local level of turbulence due to the experimental procedure. Further experiments are planned for investigating this last point.

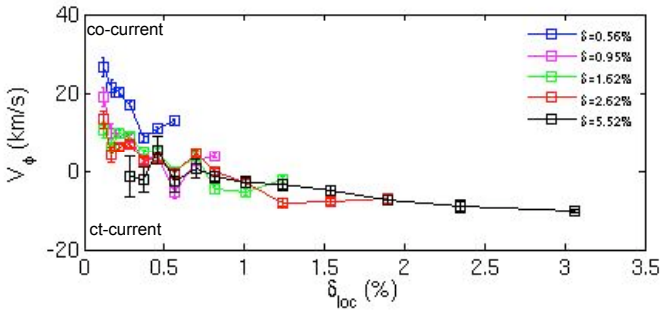

Figure 9: Toroidal rotation vs. local value of ripple amplitude.

Characterization of Micro-turbulence. Taking advantage of Tore Supra unique set of turbulence measurement, characterisation of micro-turbulence has been performed during dedicated dimensionless scans. Especially, the impact of changing ν^* on wavenumber spectrum has been investigated using a Doppler backscattering system [27]. These high resolution measurements yield perpendicular wavenumber (k) spectrum the global shape of which is a robust feature for various plasma conditions. Such spectra are well fitted by considering two regions: the first one ($k \bullet \rho_s < 0.7$), corresponding to a region of energy injection from the main instabilities, is well represented by a Gaussian function, $A \bullet e^{-\xi k^2}$; the second one ($k \bullet \rho_s > 0.7$), corresponding to a region of energy transfer, is well described by the simple expression $A \bullet k^{-3}/(1+k^2)^2$ obtained from the spectral shell model for drift waves [28,29] in the case where disparate scale interactions, in particular interaction with large scale structures as zonal flows (ZF) and geodesic acoustic modes [34], are dominant. It is worth noting that the shell model expression does not have any fitting parameters (apart from the fluctuation level). Therefore, the agreement between experiment and this model is remarkable and suggests that interaction between fluctuations and large scale structures is an important ingredient to determine the wavenumber spectrum shape in the energy transfer region. Contrary to the high k region in which no significant change of the spectra shape is observed during the dedicated ν^* experiments, the low k region exhibits faster decrease with decreasing collisionality: when decreasing collisionality by a factor of 4, the fitting parameter of the Gaussian ξ varies from 1.6 to 3.3, for spectra measured at a normalized radius (ρ) of 0.8. This observation does not support explanations based on standard effect of collisionality on ZF and/or

Trapped Electron Mode (TEM). On one hand, it is expected that a decrease of ν^* would reduce the damping on ZF, which would lead to a decrease of energy content on small wavenumbers due to the shearing by large scale structures. This would give a flatter wavenumber spectrum when decreasing ν^*. On the other hand, considering the role of TEM, the increase of ν^* is supposed to stabilize TEM and then is expected to peak the spectrum (since only the Ion Temperature Gradient "peak" remains).

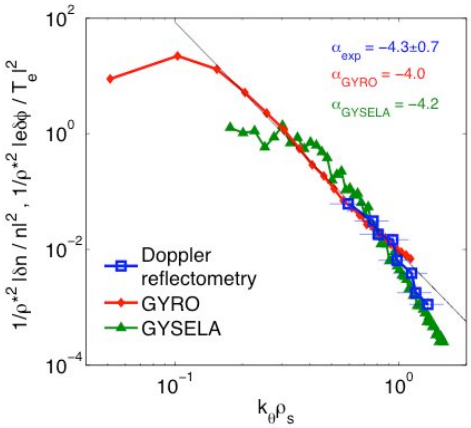

Figure 10: Experimental density fluctuation spectrum (poloidal direction) and comparison with GYRO and GYSELA predictions.

Experimental validation of gyrokinetic non linear simulations of turbulence. The understanding of turbulent fluctuations in the core of tokamak plasmas, causing a degradation of the confinement, is a crucial issue in view of future fusion reactors. Global empirical scaling laws are often used to extrapolate the performance of the next generation devices. However, predictive capabilities should rely on first principle models comprehensively retaining the relevant physics. Experimental validation of such models is an essential step toward this aim. For this purpose, Tore Supra is particularly well suited, thanks to its comprehensive set of reflectometers allowing measuring turbulence spectra both in radial and poloidal direction. Using the parameters of discharge #39596, non linear simulation of micro turbulence has been performed with the local (flux tube) gyrokinetic Maxwell code GYRO [30]. For the first time, numerical results simultaneously match within experimental uncertainty the magnitude of i) effective heat diffusivity (experimentally obtained from a power balance analysis using the CRONOS code [31]), ii) rms values of density fluctuations (measured with a fast sweeping reflectometer [32]),wave-number spectra in the iii) radial (fast sweeping reflectometer) and iv) poloidal (Doppler reflectometer [27]) direction. Figure 10 displays the poloidal density fluctuations spectrum at r/a = 0.7 obtained with the Doppler reflectometer, in agreement with GYRO predictions. An excellent agreement is also obtained with simulation with the full-f global 5D gyrokinetic code GYSELA [33]. In this global simulation, the spectral power density at low poloidal wave number is flatter, likely due to the presence of large scale sheared flows in the frequency range of geodesic acoustic modes [34]. However, at higher wave number, the non linear cascades leads to spectra similar to the measured and the local GYRO ones. This evidence suggests that, in tokamak plasmas, the turbulence wave-number spectrum exhibits a rather general character, likely governed by the dominant nonlinearities in the system, namely, the E × B convection terms.

Electron Temperature Gradient Dependence of Heavy Impurity Transport. The influence of the normalized electron temperature ($R/L_{Te} = -R \bullet \nabla T_e/T_e$) gradient on impurity transport has been studied by varying the power deposition location of electron cyclotron resonant heating (ECRH) into sawtooth- and MHD-free Tore Supra plasmas in which nickel (Ni) has been injected by the laser blow-of technique. The impurity diffusion coefficient D and convective velocity V radial profile have been determined using the ITC code [35]. For a given D and V profile, the ITC code solves the system of continuity equations coupling all the ionization stages of Ni and synthesizes signals from VUV spectroscopy and soft-X-ray cameras. Using the results from ITC, a minimization procedure based on the genetic algorithm PIKAIA [36] is applied and yields the D and V profiles that best fit the experimental data. In two discharges the same ECRH power (250 kW) is injected in different locations: $\rho = 0.35$; $\rho = 0.6$. In a third discharge the same power is equally distributed between these two locations. In the three cases, the whole V profile and the outward part ($\rho>0.3$) of the D profile are similar within error bars. However, in the core part of the plasma ($\rho<0.2$), D increases as the power deposition location moves outward. Reporting these results to R/L_{Te} variation, a steep

increase of D is observed at ρ = 0.1 (see Figure 11) while no strong variation is observed at ρ = 0.4 (3 m^2s^{-1} < D < 4 m^2s^{-1} for 8 < R/L_{Te} <12). Figure 11 strongly suggests the existence of a critical T_e gradient above which turbulent transport develops, even if it was not possible reaching low enough value of R/L_{Te} to directly observe it. Linear gyrokinetic modelling of these discharges with the GYRO code [30] shows the existence of two regions: in the inner part of the plasma (ρ<0.15), turbulence is found to be dominated by modes in the electron drift direction like TEM, which depend on ∇T_e; further out (ρ>0.25), turbulence is dominated by ion temperature gradient modes independent of T_e. The dependence of D with R/L_{Te} has been computed with the quasilinear gyrokinetic fixed-gradient code QUALIKIZ [37], that when renormalized by a single factor, reproduces well nonlinear GYRO results [38]. In fair agreement with extrapolation of the experimental data, the simulation result exhibits a threshold (R/L_{Te} ~6) above which impurity turbulent transport appears.

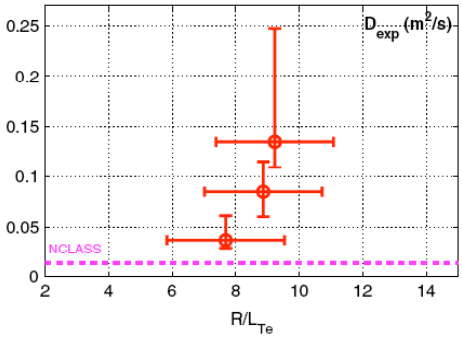

Figure 11: D vs. R/L_{Te} at ρ = 0.1.

Dynamic of Turbulence in the Plasma Edge. Understanding transport phenomena taking place at the edge of tokamak plasmas is of crucial importance since they influence directly or indirectly discharges performance: the convection of plasma filaments is considered as the dominant transport mechanism controlling the heat and particle loads on the plasma facing components and is presumably involved in the density limit phenomena; the near-sonic parallel flows observed in the SOL, influence the impurity migration, define potentially strong boundary conditions for core plasma rotation and seem to affect the L to H-mode power threshold. By correlating data from fast imaging camera and reciprocating Langmuir probes, a consistent multi-facet understanding of the turbulent transport at the edge begin to emerge from experiments conducted on Tore Supra. Plasma filaments are unambiguously observed by fast imaging to propagate both in the scrape-off layer *and* inside the confined region, showing they are not a consequence of the open field line topology. Independently of their radial location, these filaments are mainly present in the low field side of the plasma and have a finite parallel extent from that region, inferring a decoupling of the HFS turbulence with the LFS as already observed on other tokamaks [39]. This LFS/HFS asymmetry has been confirmed by a poloidal mapping of the radial particle flux derived from reciprocating Mach probe measurements: indeed, by interpreting the near sonic parallel flow at the probe location as a return flow balancing the particle source asymmetry with respect to the pressure balance, it is possible to estimate the radial flux, at the probe radial position, integrated along the magnetic field line connecting the probe to a limiter [40]. When using the toroidal pump limiter (TPL) situated at the bottom of Tore Supra, more than 85 % of the flux is found being distributed on the LFS. By inserting a secondary limiter located at the outboard mid-plane and varying the contact point along its poloidal extension, one can then refined the shape of the poloidal distribution of the radial flux. Figure 12 shows that a Gaussian distribution of the flux centred on the outboard mid-plane and with a

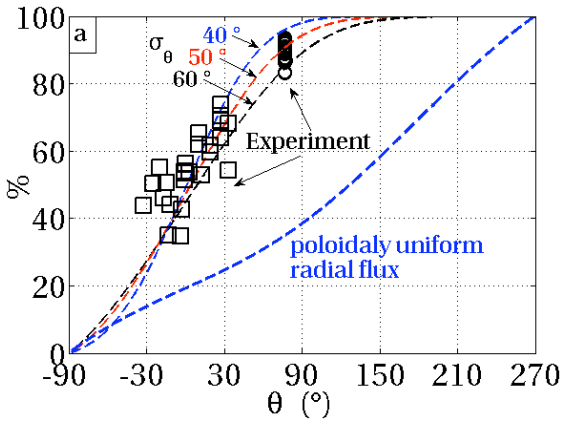

Figure 12: fraction of radial flux integrated along the magnetic field line connecting the TPL to the secondary limiter (square) or probe location (circle) vs. the poloidal position of the secondary limiter contact point or probe. Dashed line corresponds to reconstruction using Gaussian radial flux centred on the outboard midplane.

poloidal half width of about 50% fits well the experimental distribution. Finally, electrostatic fluctuations have been measured with a poloidal rake probe situated at the plasma top and reveals radial E×B convection of density bursts with a net positive time averaged flux value that is coherent with an outward propagation of filamentary structures. It is worth to note that radial flux estimated from turbulence measurements at the rake location (2 10^{20} m^2s^{-1}), is in fair agreement with the one deduced from the poloidal mapping. These observations put together yield an indirect but coherent picture of transport processes involved in the SOL: interchange instabilities make plasma filaments born at the outboard mid-plane with a finite parallel extent. Their electrostatic convection results in a radial flux highly localised in the low field side. As a consequence of this flux asymmetry, near-sonic parallel flows are driven to balance the pressure along field lines from the low to the high field side.

6. Conclusion

Since the last AIEA conference, the programme of Tore Supra has focused on physics, operation and technological issues essential for the consolidation of design choices and efficient exploitation of ITER. Thanks to the unique long pulse capability of Tore Supra, a new LHCD launcher, based on the PAM concept, has been successfully tested on long duration plasma discharges. Conceived for being able to cope with ITER neutron load, the PAM concept has demonstrated its capabilities for efficient cooling, long distance coupling and power density handling consistent with the design value foreseen for an ITER LHCD system. Progress have been made on real time control of plasmas, featuring development of "search and maintain" algorithm for control of stationary states of the current profile and destabilization of sawteeth in the presence of a significant fast ion pressure inside the q=1 surface. A new scaling law has been derived for the parallel power decay length in the SOL, a crucial point for determining the power deposition during the L-mode ramp-up phase of ITER before the X-point formation. Disruption mitigation studies by massive gas injection have evidenced the role of the q = 2 surface in limiting the gas penetration, an important information for extrapolation of MGI to ITER. The capability of recovering from disruption using ion cyclotron wall conditioning in the presence of a permanent magnetic field has been demonstrated.

Significant results have also been obtained on more fundamental issues. Concerning the intrinsic plasma rotation, a subject of importance for ITER, the competition between turbulent transport processes and ripple toroidal thermal friction has been clearly observed. The unique set of turbulence diagnostics of Tore Supra has allowed the characterization of the effect of collisionality on micro turbulence and the experimental validation of gyrokinetic non linear codes, with for the first time numerical results simultaneously matching the magnitude of effective heat diffusivity, rms values of density fluctuations, and wave-number spectra. A clear correlation between electron temperature gradient and impurity transport in the very core of the plasma has been established, strongly suggesting the existence of a threshold above which transport is dominated by turbulent electron modes. Dynamics of edge turbulent fluctuations has been studied by correlating data from fast imaging cameras and Langmuir probes, yielding a coherent picture of transport processes involved in the SOL.

Because realizing high power/long duration discharge asks for a comprehensive integration between physics and technology, the Tore Supra programme naturally encompasses many issues of importance for ITER, ranging from fundamental physics to operational issue and technological tests. The contribution of the Tore Supra programme to ITER will even be amplified with the completion of the CIMES project that will allow, not only to test technological objects in more stringent conditions but also to extend the operational domain of long-duration discharges to higher plasma current and densities.

Acknowledgements. This work, supported by the European Communities under the contract of Association between EURATOM and CEA, was carried out within the framework of the European Fusion Development Agreement. The views and opinions expressed herein do not necessarily reflect those of the European Commission.

[1] B. Saoutic, Plasma Phys. Control. Fusion **44** (2002) 1.
[2] D. Van Houtte *et al.*, Nucl. Fusion **44** (2004) L11.
[3] Beaumont B. *et al.*, Fusion Eng. Des. **56–57** (2001) 667.
[4] Ph. Bibet *et al.*, Fusion Eng. Des. **74** (2005) 419.
[5] V. Pericoli Ridolfini *et al.*, Nucl. Fusion **45** (2005) 1085.
[6] G.T. Hoang *et al.*, Nucl. Fusion **49** (2009) 075001.
[7] A. Ekedahl *et al.*, Proc. 18th Topical Conf. on RF Power in Plasmas, Gent. AIP Conf. Proc. **1187** (2009) 407.
[8] J. Hillairet *et al.*, Fusion Eng. Des. **84** (2009) 953.
[9] J.P. Gunn *et al.*, Journal Nuc. Mat. **390-391** (2009) 904.
[10] M. Chatelier, Nucl. Fusion, **47** (2007) S579-S589.
[11] G.T. Hoang *et al.*, Nucl. Fusion **34** (1994) 75.
[12] P. Maget *et al.*, Nucl. Fusion **44** (2004) 443.
[13] G. Giruzzi *et al.*, Nucl. Fusion **49** (2009) 104010.
[14] V. Krivenski *et al.*, Nucl. Fusion 25 (1985) 127.
[15] A. Bécoulet *et al.*, Comput. Phys. Commun. **177** (2007) 55.
[16] Kepler: .http://kepler-project.org.
[17] Scicos; http://www.scicos.org.
[18] ITER Physics Basis, Nucl. Fusion **39** (1999) 2391.
[19] J. P. Gunn *et al.,* J. Nucl. Mater. **363-365** (2007) 484.
[20] A. M. Kočan, J. P. Gunn, Plasma Phys. Control. Fusion **52** (2010) 045010.
[21] C. Reux *et al.*, accepted for publication in Nuc. Fusion
[22] C. Grisolia *et al.*, Vacuum **60** (2001) 147.
[23] C. Fenzi *et al.*, submitted to Rev. Sci. Instrum.
[24] M.F.F. Nave. *et al.*, Phys. Rev. Lett. **105** (2010) 105005.
[25] M. Yoshida *et al.*, Plasma Phys. Cont. Fusion **48** (2006) 1673.
[26] X. Garbet *et al.*, Phys. Plasmas **17** (2010) 072505.
[27] P. Hennequin *et al.*, Nucl. Fusion **46** (2006) S771.
[28] Ö. D. Gürcan *et al,* Phys. Rev. Lett. **102** (2009) 255002.
[29] Ö. D. Gürcan *et al.,* Plasma Phys. Cont. Fusion **52** (2009) 045002.
[30] J. Candy and r. E. Waltz, Phys. Rev. Lett. **91** (2003) 045001.
[31] V. Baziuk *et al.*, Nucl. Fusion, **43** (2003) 822.
[32] F. Clairet *et al.*, Plasma Phys. Cont. Fusion **43** (2001) 429.
[33] V. Grangirard *et al.*, Plasma Phys. Cont. Fusion **49** (2007) B173.
[34] K. Hallatschek and D. Biskamp, Phys. Rev. Lett. **86** (2001) 1223.
[35] R. Guirlet *et al.*, Nucl. Fusion 49 (2009) 055007.
[36] P. Charbonneau, Astrophys. J. Suppl. Ser. **101** (1995) 309.
[37] C. Bourdelle *et al.*, Phys. Plasmas **14** (2007) 112501.
[38] A. Casati *et al.*, Nucl. Fusion **49** (2009) 085012.
[39] J. L. Terry *et al.*, Physics of Plasma **10** (2003) 1739.
[40] N. Fedorczak *et al.*, submitted in Journal of Nuclear Materials.